

# SELECTING A SQUEEZE FILM DAMPER MODEL FOR SOLVING ROTOR DYNAMICS GTE PROBLEMS

© 2017

**Leontiev Mikhail K.** Doctor of science (Technical), Professor of 203 department «Construction and design of engines»;  
Moscow aviation institute (national research university);  
[lemk@alfatran.com](mailto:lemk@alfatran.com)

**Kutakov Maksim N.** software engineer;  
Engineering & consulting centre for dynamic problems in rotating machinery Alfa-Transit, Co. Ltd.;  
[maxim.kutakov@alfatran.com](mailto:maxim.kutakov@alfatran.com)

Various standard mathematical squeeze film damper (SFD) models, which can be applied for solving rotor dynamics problems of gas turbine engines (GTE), are presently available. Accuracy of the whole simulation is ultimately affected by the choice of a certain SFD formulation, which depends on many factors – geometry parameters, oil supply method, oil inlet pressure, operating conditions etc. The present contribution suggests some recommendations for selecting a particular mathematical SFD model and compares the simulation results obtained with different SFD formulations. To this end a point rotor system is numerically analyzed with the aid of the DYNAMICS R4 (www.alfatran.com) software.

*GTE; rotor system; squeeze film damper, mathematical modeling.*

## Nomenclature

$p$  - local pressure, Pa;

$R$  - damper radius, mm;

$D = 2R$  – damper diameter, mm;

$L_{eq}$  - equivalent damper length  $L_{eq} = \sqrt[3]{4(L_1^3 + L_2^3)}$ , mm;

$\varepsilon$  –eccentricity ratio;

$\rho$  – oil specific mass, kg/m<sup>3</sup>;

$e$  – eccentricity, mm;

$\Omega$  – rotor precession frequency, sec<sup>-1</sup>;

$\mu$  – oil dynamic viscosity, Pa\*sec;

$c$  – radial gap, mm;

$P_p$  –oil supply pressure, Pa;

$P_N$  –saturated vapor pressure, Pa;

$\bar{P}_p = \frac{c^2 P_p}{12\mu\Omega R^2}$  – dimensionless oil supply pressure;

$\bar{P}_n = \frac{c^2 P_n}{12\mu\Omega R^2}$  – dimensionless saturated vapor pressure;

$\bar{P}_k = \bar{P}_n (R/L)^2$  – dimensionless oil supply rate;

$\bar{P}_N = \bar{P}_p - \bar{P}_n$  ;

$A_K, B_K$  – cavitation parameter of a “short” open ends damper;

$A_K = 1 + (3.76(1 - \varepsilon)^{1.51} \exp[2.89(1 - \varepsilon)])\bar{P}_K$ ,

$B_K = 1 - (10.2(1 - \varepsilon)^{2.24} \exp[1.88(1 - \varepsilon)])\bar{P}_K$ ,

$A_D$  – cavitation parameter of a “long” damper;

$$A_D = 1 + 4 \times 10^{-5} (1 - \varepsilon)^{6.12} \exp[12.9(1 - \varepsilon)] \bar{P}_N^{-0.9}, \quad \text{at } 0 < \varepsilon < 0.5;$$

$$A_D = 1 + (2.76 - 2.45\varepsilon) \bar{P}_N^{-0.75}, \quad \text{at } 0.5 < \varepsilon < 0.9,$$

$$\Omega_* = \frac{c^2 \Omega \rho}{\mu} - \text{reduced oscillation frequency};$$

$$Re = \frac{\rho R \Omega e}{\mu} - \text{Reynolds number.}$$

## Introduction

Supports of many Gas Turbines (GT) are equipped with squeeze film dampers (SFD). Viscous friction in dampers dissipates the rotor vibration energy and thus reduces the vibration magnitudes. Computer simulation of rotor system dynamic response, specifically of the damper supports, is an important stage of a GT design.

Various computer simulators for dampers are available nowadays. The simulation models are based on analytic, or numerical solutions of fluid flow equations for the damper gap. Theoretical aspect of these solutions is well known [1], [2], [3] but a practical model choice usually causes problems. This paper considers choice of the damper model that is directly concerned with the damper design and the GT operating conditions.

### Analytic models for squeeze film dampers

The damper may be presented as a mechanical system with two degrees of freedom, the oscillator is in relative motions in the circular direction (precession motion) and in the radial one, angular misalignment in the axial direction is absent. All forces in the damper are shown in figure 1.

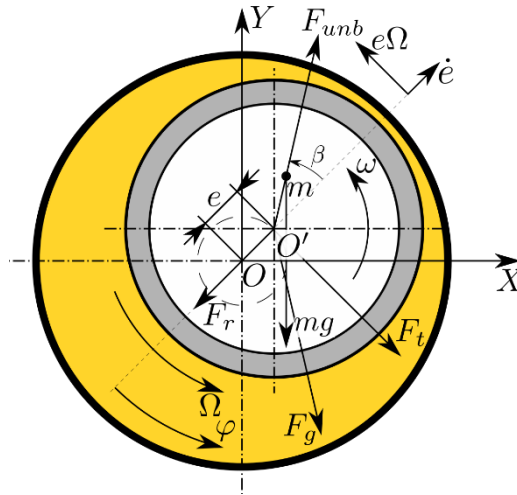


Fig. 1. Unbalance and resistance loads in the damper.

The damper resistance forces may be calculated by the dynamic pressure integral over the oscillator surface area. In the local coordinate system  $r, t$ :

$$\bar{F} = \{F_r, F_t\}; \quad (1)$$

$$F_r = -R \int_0^{2\pi} \int_0^L p \cos(\varphi) d\varphi dz; \quad (2)$$

$$F_t = -R \int_0^{2\pi} \int_0^L p \sin(\varphi) d\varphi dz.$$

The pressure distribution in the oil film may be obtained from the Reynolds equation solution [4] that takes into account the oil pressure gradients in circular and axial directions. In these terms the Reynolds equation may be considered as a 2-D SFD model. The Reynolds equation has no analytical solution and may be solved by a numerical method.

The equation may be reduced to the 1-D approach by application of “short” or “long” damper models combined with the cavitation conditions, either Gumbel condition, or the  $\pi$ -film where the oil covers a half of the journal circle, or Sommerfeld condition, or the  $2\pi$ -film where the damper surface is completely coated with oil, which the cavitation absence. This approach allows the pressure function analytic presentation. Further this approach gives analytic calculation of the damper forces caused by the oscillator motion (ref table 1) [2].

Table 1. Analytic equations for the damper forces in rotating coordinates

“Short” damper	
$\pi$ -film	$2\pi$ -film
$F_r = \mu R \frac{L^3}{c^2} \left[ \frac{\pi}{2} \frac{1+2\varepsilon^2}{(1-\varepsilon^2)^{5/2}} \dot{\varepsilon} + \frac{2\Omega\varepsilon^2}{(1-\varepsilon^2)^2} \right]$	$F_r = \pi\mu R \frac{L^3}{c^2} \frac{1+2\varepsilon^2}{(1-\varepsilon^2)^{5/2}} \dot{\varepsilon}$
$F_t = \mu R \frac{L^3}{c^2} \left[ \frac{2\varepsilon\dot{\varepsilon}}{(1-\varepsilon^2)^2} + \frac{\pi}{2} \frac{\Omega\varepsilon}{(1-\varepsilon^2)^{3/2}} \right]$	$F_t = \pi\mu R \frac{L^3}{c^2} \frac{\Omega\varepsilon}{(1-\varepsilon^2)^{3/2}}$
”Long” damper	
$\pi$ -film	$2\pi$ -film
$F_r = 6\mu L \frac{R^3}{c^2} \left[ \frac{\pi\dot{\varepsilon}}{(1-\varepsilon^2)^{3/2}} + \frac{4\Omega\varepsilon^2}{(2+\varepsilon^2)(1-\varepsilon^2)} \right]$	$F_r = 12\pi\mu L \frac{R^3}{c^2} \frac{\dot{\varepsilon}}{(1-\varepsilon^2)^{3/2}}$
$F_t = 12\mu L \frac{R^3}{c^2} \left[ \frac{2\dot{\varepsilon}}{(1-\varepsilon)(1-\varepsilon^2)} + \frac{\pi\Omega\varepsilon}{(2+\varepsilon^2)(1-\varepsilon^2)^{1/2}} \right]$	$F_t = 24\pi\mu L \frac{R^3}{c^2} \frac{\Omega\varepsilon}{(2+\varepsilon^2)(1-\varepsilon^2)^{1/2}}$

The analytic equations may be applied within a range of the damper dimensions where the “short” and “long” damper assumptions are adequate. Besides this the analytic approach roughly considers the cavitation effect, the oscillator oil coating is either complete in the  $2\pi$ -film or the half circle coating in the  $\pi$ -film. Nevertheless these approaches are widely used. The theoretic limits for the analytic approach applications [5] are summarized in table 2.

If the model considers a finite length damper, or oil supply pressure, or the gap flow turbulence, or inertia forces, or accurate cavitation models, etc. the solution must apply computational methods to the modified 2-D Reynolds equation. The computer approach needs much more computation time but the results are more accurate in the cases where the analytic equation assumptions produce large errors.

Table 2. limits for the models application

<b>Flow mode</b>		
Laminar		Turbulent
$Re < 1200$		$Re > 1200$
<b>Calculation method</b>		
“Short” damper	Finite length damper	“Long” damper
$L/D < 0.5$ $\varepsilon \leq 0.75$	$0.5 < L/D < 2$	$L/D > 2$
<b>Inertia forces consideration</b>		
Convective		Temporal
$\Omega_* > 10$		$\Omega_* > 1$ , unsteady solution
<b>Cavitation model</b>		
$\pi$ - film	Specific approach	$2\pi$ -film
$A_K(A_D) < 1.1$	$1.1 < A_K(A_D) < 2$	$A_K(A_D) > 2$

### Simulation of a rotor with a flexible damper support

The model comprises a point rotor, a housing system and links between them as shown in figure 2.

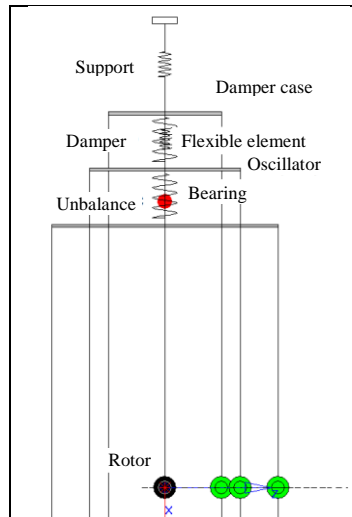


Fig. 2. Simulation of a point rotor with a flexible damper support in DYNAMICS R4 code.

The links simulate a bearing, a non-linear squeeze film damper, a flexible element and a support. The rotor system model parameters are presented in Table 3.

Table 3. Rotor system model parameters

Parameter	Value
Housing mass, kg	100
Support stiffness, N/m	$5e+9$
Bearing stiffness, N/m	$5e+8$
Flexible element stiffness, N/m	$1e+7$
Support damping, N*sec/m	2000
Bearing damping, N*sec/ m	500
Rotor mass, kg	25
Oscillator mass, kg	5
Rotor speed, rpm	8000
Rotor unbalance, g*cm	50

The rotor first critical speed without the damper influence is 5470 rpm, the damper forces taken into account will change this value.

The example damper taken from a real GT is shown in figure 3. The damper has a central oil supply groove and end seals. The damper is unloaded, or centralized by a “squirrel cage” type flexible element.

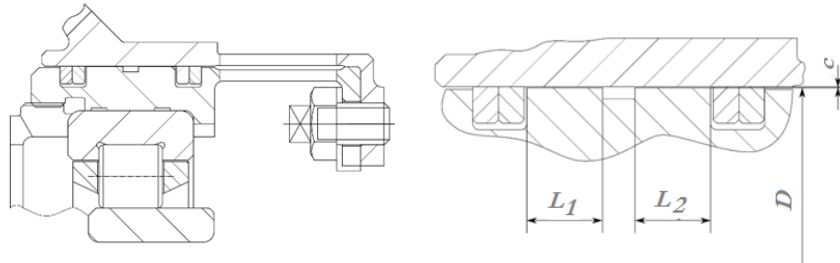


Fig. 3. SFD with a flexible element in a GT structure.

The damper initial parameters are given in table 4. The end seals are considered as ideal, without leakages (zero flow damper). The oil pressure in the groove is taken constant in all directions and equal to the supply pressure. [6].

Table 4. Damper parameters

PARAMETER	value
Damper radius, mm	84
Oil supply groove location	Central
Damper length (groove included), mm	18
Groove width, mm	3
Radial gap, mm	0.15
Oil name	MC-8II
Oil temperature, °C	60
Oil dynamic viscosity, Pa*sec	0.00513
Oil specific weight, kg/m <sup>3</sup>	845
Oil supply pressure, bar	4

### Algorithm for the damper model choice

For the centered damper the analytic solutions of Reynolds equations may be applied regardless to the oil supply design, groove or orifices. Here we clarify the conditions that allow application of the analytic solutions to the rotordynamics problems.

Algorithm of choice of the damper model is disclosed by the damper example with parameters given in table 4. Criteria of table 2 may be calculated through the relative eccentricity  $\varepsilon$  at the given speed, here 5470 rpm. This needs a preliminary calculation in the unsteady approach and the adequate model tuning. After the eccentricity is obtained the model tuning may be refined. The preliminary calculated eccentricity value is  $\varepsilon = 0.73$ . Steps of this algorithm and the calculation results are given in table 5.

Table 5. Algorithm for the choice of damper model

Step	Calculated parameter	Calculation result	Choice parameter
1	$L/D$	$L_{eq} = 15 \text{ mm}; L/D = 0.09 < 0.5$	“short”
2	Choice of cavitation model	$A_K = 2.29 > 2$	“ $2\pi$ – film”
3	Convective member of inertia forces	$\Omega_* = 2.12 < 10$	Not needed
4	Temporal member of inertia forces	$\Omega_* = 1 < 2.12$	Needed
5	Turbulence consideration	$Re = 868 < 1200$	Not needed

The applied non-linear damper model in the DYNAMICS R4 system library does not take into account the oil inertia. The algorithm shows that the temporal inertia member must be involved. On the other hand, when the subject is a specific rotation speed the local inertia members may be neglected.

In this example results of different analytic models application may be compared with the results of numerical solutions that calculate more accurately the flow performance, especially the cavitation conditions. In the numerical 2-D damper model the mesh has 90 nodes in the circular direction and 28 nodes in the axial one. The mesh density provides sufficient solution accuracy for all boundary conditions.

The rotor and damper parameters influence the model choice. The analysis subject is the rotor motion under the weight and unbalance loads during the rotor acceleration. The calculation results are frequency response of the peak-to-peak motion amplitude in the vertical direction and the motion orbits at a given rotation speed.

**Oil supply pressure 4 bar.** It is worth saying that in the case of 1-D analytic model the oil supply pressure is taken into account indirectly through the calculated parameter  $A_K, A_D$ . Based on this parameter value the vibrator is considered as completely or half coated with oil. In the numerical 2-D model the oil supply enters the calculation directly through the boundary conditions.

The damper (ref. the table 4 parameters) is aligned by the flexible support and the unbalance and weight loads are of a similar order. The rotor itself location is practically near the damper gap center. This design is typical for the aviation GTs. The calculation results are shown in figure 4.

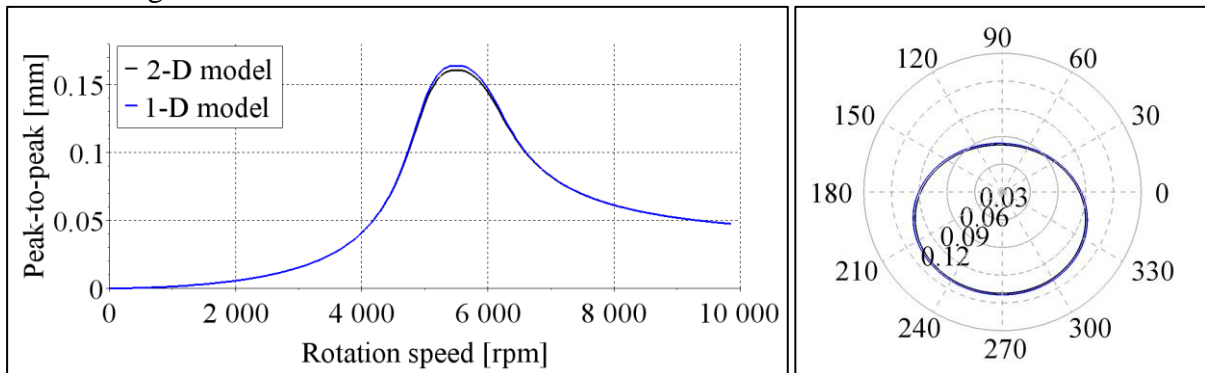


Fig. 4. Rotor oscillation peak-to-peak magnitude and orbit at resonance frequency  
The orbits obtained from the 1-D damper model and the 2-D one are practically equal.

**Oil supply pressure lowered down to 0.1 bar.** Calculation with the proposed algorithm show the following results:  $L_{eq} = 15$  mm – the “short” damper model,  $Re = 1095 < 1200$  - turbulence may be not considered,  $A_K = 1 < 1.1$ - the  $\pi$ - film model may be applied,  $\varepsilon \approx 0.8$  and  $\Omega_* = 2.45 < 10$  - convective inertia forces may be not considered. The results are shown in figure 5.

The lower oil pressure produced an instantaneous decrease of the magnitude right after the resonance frequency, the so-called “jump-effect”. The resonance frequency moved from 5470 rpm in the base model to ~6300 rpm, the damping also dropped.

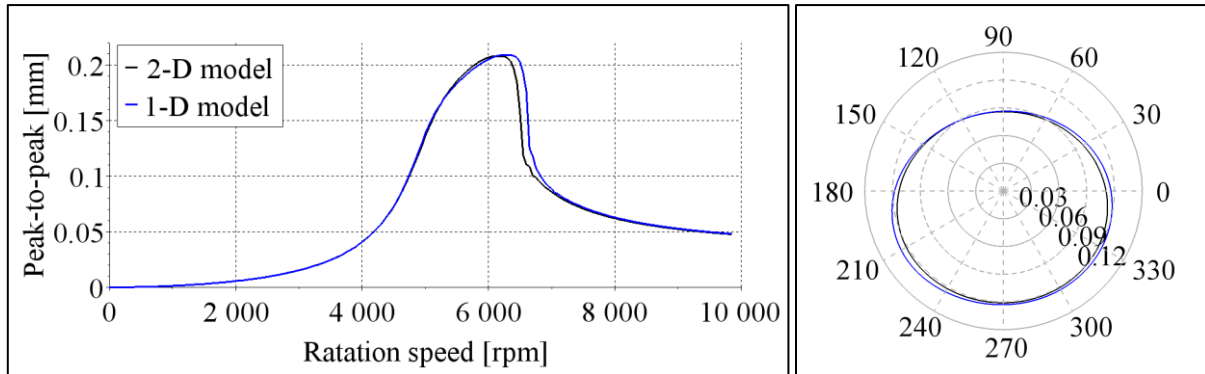


Fig. 5. Rotor oscillation peak-to-peak magnitude and the resonance frequency orbit at lower oil supply pressure

The numerical model calculation results are mostly similar to the analytic ones.

**Lower unbalance value.** This configuration may occur in industrial and marine GT. Here we consider the 5 gcm unbalance which is 10 times smaller than the base model one and the base model oil supply pressure 4 bar. . The preliminary calculation shows that the precession magnitude is smaller than the static rotor deflection produced by its weight. The precession occurs around a steady state location.

The proposed algorithm calculations show the following results:  $L_{eq} = 15$  mm – “short” damper model,  $Re = 381 < 1200$  - turbulence is negligible,  $A_K = 18 > 2$  -  $2\pi$  - film may be applied. At the resonance frequency ~5600 rpm  $\varepsilon \approx 0.3$ ;  $\Omega_* = 2.17 < 10$  - the convective inertia forces may be omitted. The calculation results are given in figure 6.

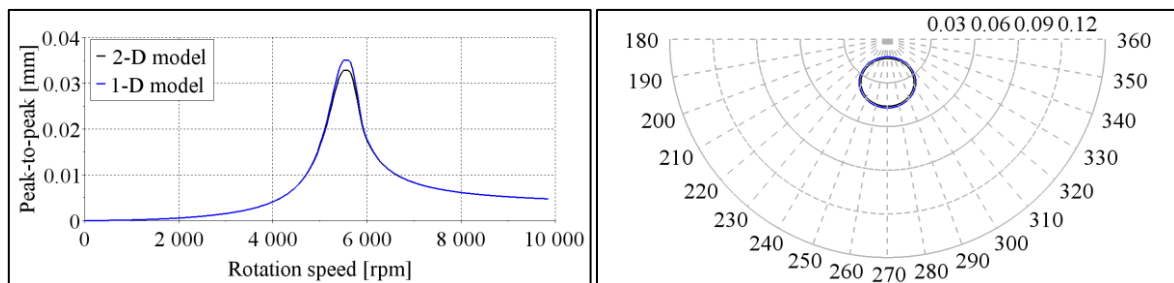


Fig. 6. Rotor oscillation peak-to-peak magnitude and the resonance frequency orbit at lower unbalance load.

The numerical model calculation results are similar to the analytic model ones. The unbalance load cannot produce the spinning motion (the nearly circular motion around the geometrical rotor axis), damping in this case is minimal.

**Another location of the oil supply groove.** Consider the base model damper but with the oil supply groove moved to the utmost right location (ref. figure 7).

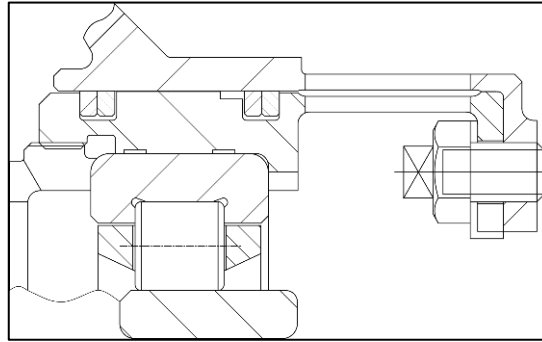


Fig. 7. The oil supply groove moved from the mid-span,

For this damper  $L_1 = 15$ ,  $L_2 = 0$ . The proposed algorithm calculations show the following results:  $L_{eq} = 23.8$  mm – “short” damper model,  $Re = 602 < 1200$  - turbulence is negligible,  $A_K = 3.7 > 2 - 2\pi$  - film mode may be applied,  $\varepsilon \approx 0.478$ ;  $\Omega_* = 2.25 < 10$  – the convective inertia forces may be omitted. The calculation results are shown in figure 8.

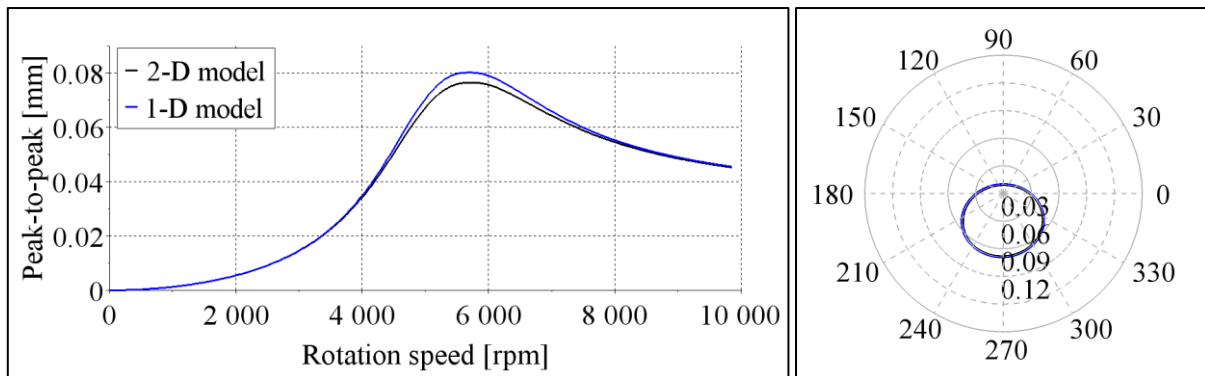


Fig. 8. Rotor oscillation peak-to-peak magnitude and the resonance frequency ~5800 rpm orbit with the oil supply groove moved.

The groove displacement increases the damper equivalent length and produces a higher damping force, the resonance frequency magnitude becomes smaller. The resonance frequency is almost equal to the base model one. The analytic and numerical models show similar results because the first model is applied within its limits.

**Oil supply through orifices.** Dampers with oil supply through orifices have specific features of performance and calculation procedure. In the example oil is supplied through 4 equally spaced 5 mm diameter orifices. In this case the axial direction pressure gradient is small, except the orifice vicinity, so the “long” damper model is assumed.

The example damper parameters are the following: damper length  $L = 15$  mm – the “long” damper model,  $Re = 369 < 1200$  - turbulence neglected,  $A_D = 1.017 < 1.1 - \pi$  - film model,  $\varepsilon \approx 0.17$ ;  $\Omega_* = 3.88 < 10$  - convective inertia forces may be neglected. The  $L/D > 2$  condition of table 2 is not fulfilled. The calculation results are shown in figure 9.

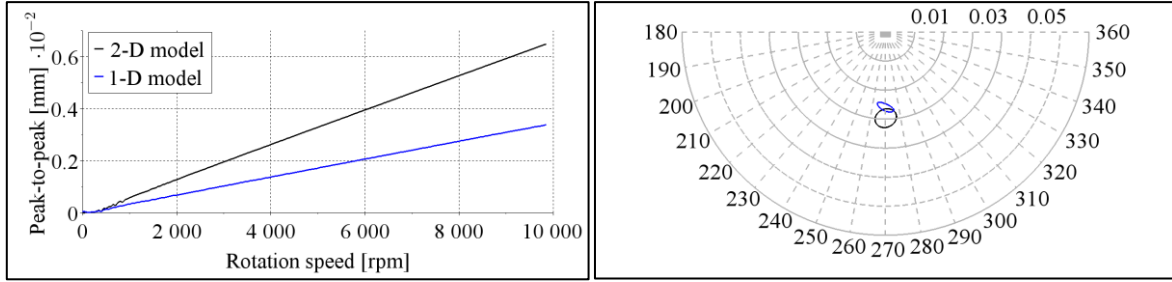


Fig. 9. Rotor oscillation peak-to-peak magnitude and the ~10000 rpm frequency orbit with the oil supply through orifices.

The 1-D and 2-D models calculation results differ about two times throughout the whole speed range. First of all this may be explained by the rough cavitation evaluation in the 1-D model. It is worth mentioning that the  $A_D$  and  $A_K$  evaluations are concerned with circular centered orbits which may produce errors in the case of misaligned orbits. Besides, this oil supply method changes the gap flow distribution which cannot be reflected by 1-D models, and the 2-D labor consuming model results are more accurate

**Noncentered damper with the mid-span oil supply groove.** All examples above analyze the usually applied in GT supports centered dampers. Below are considered specific features of noncentered dampers.

The noncentered dampers have remarkably non-linear performance but they are used by many leading GT manufacturers because of simple design and compact structures [7, 8].

When the centering (parallel retaining spring) element is absent a small static load easily moves the oscillator towards the housing wall. Thus the noncentered dampers operate at large eccentricities  $\varepsilon > 0.75$ . At these eccentricity values the support damper is very high, the magnitude is small and the motion orbit has a specific flattened form extended in circular direction, or the “crescent shape” which is experimentally observed [9, 10].

Application of analytic Reynolds equation solutions in this case may cause considerable errors. At eccentricity values  $\varepsilon > 0.9$  the friction mode changes from the hydrodynamic lubrication to the mixed-film lubrication when the surface roughness tenants get in contact. Also the housing and oscillator deformations become comparable with the gap. The models below ignore these effects. The mixed-film lubrication and elastic-hydrodynamic contact form a special investigation subject. Below are compared 1-D and 2-D damper models in absence of the centering element.

The damper model shown in figure 2 becomes noncentered after the centering link is deleted. All other model and damper parameters summarized in tables 3 and 4 are retained.

The preliminary calculation shows that at the 10000 rpm rotation speed the precession frequency is only 1183 rpm and the relative eccentricity  $\varepsilon \approx 0.9$ . The proposed algorithm calculation gives the following results:  $L_{eq} = 15$  mm – “short” damper model,  $Re = 231 < 1200$  - turbulence may be neglected,  $A_K = 1.81 > 1.1$  - the  $\pi$ -film and  $2\pi$ - film models are out of application range, a 2-D calculation is needed.

This large eccentricity causes the film discontinuity, so the  $\pi$ -film may be adequate. The parameter  $\Omega_* = 0.46 < 10$ , so the convective inertia forces may be not considered. The calculation results are shown in figure 10.

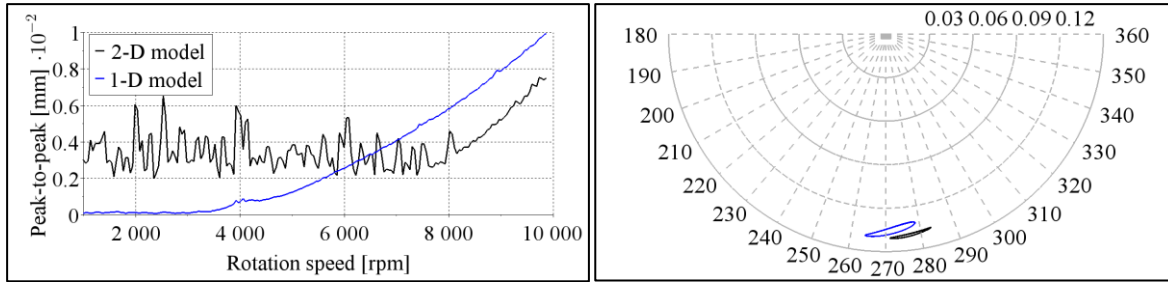


Fig. 10. The eccentric damper rotor oscillation peak-to-peak magnitude and the ~10000 rpm frequency orbit, unbalance 50 gcm.

The results show that the 1-D and 2-D models give different oscillation forms and the orbits shapes and locations.

The calculation explains the wide use of noncentered dampers. The noncentered damper at large eccentricity produces high damping, changes the rotor system dynamic performance and reduces the oscillation magnitude an order above the centered damper.

Figure 11 shows calculation results for the above example with the unbalance increased up to 100 gcm. The higher unbalance load increases the magnitude, the 10000 rpm orbits are larger. Also the two models results are nearer and the orbits tend towards circles.

The orbits are different but the main result of the analytic model, the high damping, differs not drastically which is important in practice, the practical problems may be solved in minimal computation time.

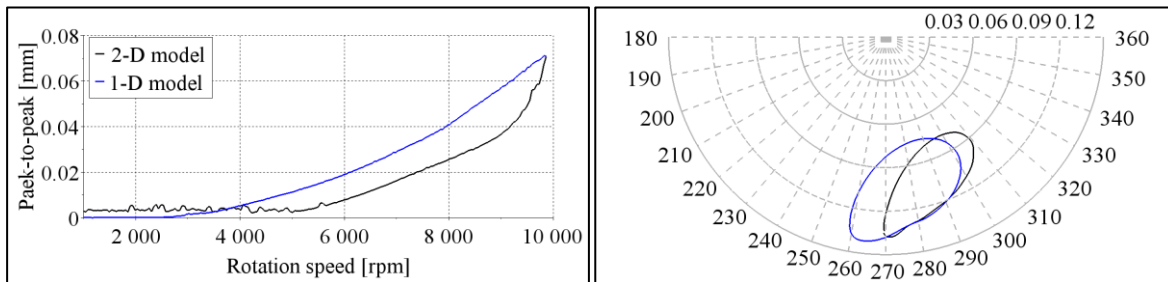


Fig. 11. The eccentric damper rotor oscillation peak-to-peak magnitude and the ~10000 rpm frequency orbit, unbalance 100 gcm.

## Conclusion

The paper discloses a method for the choice of damper model in rotor dynamics problems. The test calculation results show that the analytic damper models are near to the numerical ones within the basic assumptions limits. The analytic models calculations are labor efficient. For example, the paper shows four numerical tests where the 1-D analytic solution took about two orders less calculation time than the 2-D numeric solution. This rate remarkably depends upon the applied algorithms, problem inputs, computer model, etc. The criteria presented in the paper recommend the algorithm choice but the final methods choice is up to the engineer.

## References

1. Sergeev S. I. *Dempfirovaniye mekhanicheskikh kolebaniy* [Damping of mechanical vibrations]. Moscow: Fizmatgiz Publ., 1959. 408 p.
2. Belousov A.I., Balyakin V.B., Novikov D.K. *Teoriya i proektirovaniye gidrodinamicheskikh dempferov opor rotorov* [Theory and design of hydrodynamic rotor support dampers]. Samara: Samarskiy Nauchnyy Tsentr RAN Publ., 2002. 335 p.

3. Leontiev M. K. *Konstruktsiya i raschet dempfernykh opor rotorov GTD: Uchebnoe posobie* [Design and calculation of gas turbine engine rotor damper supports: Textbook]. Moscow: Moscow Aviation Institute Publ., 1998. 43 p.
4. Reynolds O. On the Theory of Lubrication and Its Application to Mr. Beauchamp Tower's Experiments, Including an Experimental Determination of the Viscosity of Olive Oil. *Proceedings of the Royal Society of London*. 1886. V. 40, Iss. 242–245. P. 191–203. DOI: 10.1098/rspl.1886.0021
5. Kutakov M.N., Degtiarev S.A., Leontiev M.K. Mathematical models of squeeze film dampers in rotor dynamics of gas turbine engines. *Vestnik of Samara University. Aerospace and Mechanical Engineering*. 2017. V. 16, no. 1. P. 115-128. DOI: 10.18287/2541-7533-2017-16-1-115-128
6. Marmol R.A., Vance J.M. Squeeze film damper characteristics for gas turbine engines. *Journal of Mechanical Design*. 1978. V. 100. P. 139-146.
7. Cookson R.A., Kossa S.S. The effectiveness of squeeze-film damper bearings supporting rigid rotors without a centralising spring. *International Journal of Mechanical Sciences*. 1979. V. 21, no. 11. P. 639-650.
8. Cookson R.A. Optimum design of squeeze-film damper bearings. *Proceedings of IMech*. 1981. P. 31-37.
9. Holmes R., Dogan M. Investigation of Squeeze-Film Dampers in Flexible Support Structures. *NASA Conf. Pub.* 2250. May 10 12, 1982. P. 415-433.
10. San Andrés L., Den S., Jeung S.H. Transient Response of a Short-Length ( $L/D= 0.2$ ) Open-Ends Elastically Supported Squeeze Film Damper: Centered and Largely Off-Centered Whirl Motions. *Journal of Engineering for Gas Turbines and Power*. 2016. V. 138, no. 12. P. 122503.